Excitonic and free-carrier polarizations of bulk GaAs studied by femtosecond coherent spectroscopy

Excitonic and free-carrier polarizations of bulk GaAs studied by femtosecond coherent spectroscopy

A. Leitenstorfer, A. Lohner, K. Rick, and P. Leisching
Physik Department E 11, Technische Universität München, D-85748 Garching, Germany

T. Elsaesser
Max-Born-Institut für Nichtlineare Optik und Kurzzeitspektroskopie, D-12489 Berlin, Germany

T. Kuhn
Institut für Theoretische Physik, Universität Stuttgart, D-70550 Stuttgart, Germany

F. Rossi and W. Stolz
Fachbereich Physik und Zentrum für Materialwissenschaften, Universität Marburg, D-35037 Marburg, Germany

K. Ploog
Paul-Drude-Institut für Halbleiterelektronik, D-10117 Berlin, Germany
(Received 29 December 1993)

The transient third-order polarization at the band gap of undoped and *p*-doped GaAs is investigated by spectrally and temporally resolved four-wave mixing. Excitonic and free-carrier contributions simultaneously excited within the bandwidth of the 100-fs pulses are clearly distinguished by their different spectral envelopes. The excitonic part dominates at carrier densities below 10^{16} cm^{-3} and shows a time evolution governed by exciton–free-carrier scattering and by many-body effects. At higher density, the free-carrier polarization has a strength similar to the exciton contribution and exhibits a spectrum resonant to the femtosecond pulses with a photon-echo-like temporal behavior. The data are analyzed by a numerical solution of the semiconductor Bloch equations including an ensemble Monte Carlo simulation of the scattering dynamics of the carriers. The theoretical model is in good agreement with the experimental results.

I. INTRODUCTION

Optical excitation of interband transitions in semiconductors generates a nonlinear coherent polarization which decays by phase-breaking scattering processes of the photoexcited carriers. The phase relaxation times in those condensed materials are in the femtosecond and picosecond regimes due to the strong coupling of the elementary excitations. Thus ultrafast coherent spectroscopy gives direct insight into the fundamental nonequilibrium dynamics of carrier equilibration and the concomitant dephasing processes.[1–11]

Direct-gap semiconductors show large third-order polarizations in the range of the fundamental band gap that are caused by excitons and/or free-electron-hole pairs. Techniques of degenerate four-wave mixing (FWM) with picosecond and femtosecond laser pulses have been used extensively to investigate the nonlinear polarization of bulk and low dimensional III-V semiconductors. In bulk GaAs, picosecond FWM experiments gave dephasing times of excitonic excitations as long as $T_2=7$ ps at carrier densities below 10^{14} cm^{-3}, whereas a faster loss of phase coherence by exciton-exciton collisions was observed at higher excitation levels of several 10^{15} cm^{-3}. Additional generation of free-electron-hole pairs leads to an even stronger shortening of T_2 down to $T_2<1$ ps, which was attributed to exciton–free-carrier collisions.[8]

Dephasing of electron-hole excitations in the valence- and conduction-band continua occurs on a significantly shorter time scale and—consequently—has been studied with femtosecond pulses both around the band gap $E_G\simeq 1.5$ eV and at 2 eV.[9–11] For excitation with 500-fs pulses below the threshold of LO-phonon emission, values of $T_2\simeq 300$ fs have been derived from hole burning measurements with an excitation density of 5×10^{17} cm^{-3}.[9] The rapid loss of phase coherence was attributed to collisions among free carriers. In contrast, much shorter T_2 times between 20 and 60 fs for carrier densities from 8×10^{17} cm^{-3} were extracted from measurements with pulses of $\tau=6-10$-fs duration.[10,11]

For a duration of $\tau\leq 100$ fs, the bandwidth of the pulses has a value of several tens of meV. At spectral positions close to the band gap, both excitonic and free-carrier transitions are pumped. The two types of polarizations and their interaction via many body effects should lead to significant changes of the overall nonlinear behavior compared to cases of selective excitation. For instance, the time evolution of excitonic contributions should be completely different from that of the inhomogeneously broadened continuum component.[12] These effects have been completely neglected in the analysis of previous femtosecond FWM data, where both exciton and continuum states were pumped. Very recently, we have presented a femtosecond study which provides in-

teresting information about the fundamental properties of third-order polarizations due to excitons and free carriers simultaneously excited in bulk GaAs.[13] The spectrally resolved signal in FWM experiments with 100-fs pulses provided direct insight into the nature of coherent polarizations. In this paper, we present spectrally and temporally resolved data measured with undoped as well as p-doped GaAs. In both materials, the excitonic polarization dominates at carrier densities below 10^{16} cm^{-3}, whereas an additional component due to nonthermalized free carriers is found at higher densities. The temporally resolved FWM signal gives different time behaviors for the two contributions. In addition to the experimental results, the theoretical analysis combining the solution of the semiconductor Bloch equations with an ensemble Monte Carlo simulation of the carrier dynamics is discussed in detail.

The outline of the paper is as follows. After a short description of the experimental methods in Sec. II we present experimental results measured with undoped GaAs and with p-type material (Sec. III). A qualitative discussion of the data is presented in Sec. IV, which is followed by a detailed theoretical analysis with the help of the semiconductor Bloch equations and Monte Carlo (MC) simulations (Sec. V). Finally, conclusions are presented in Sec. VI.

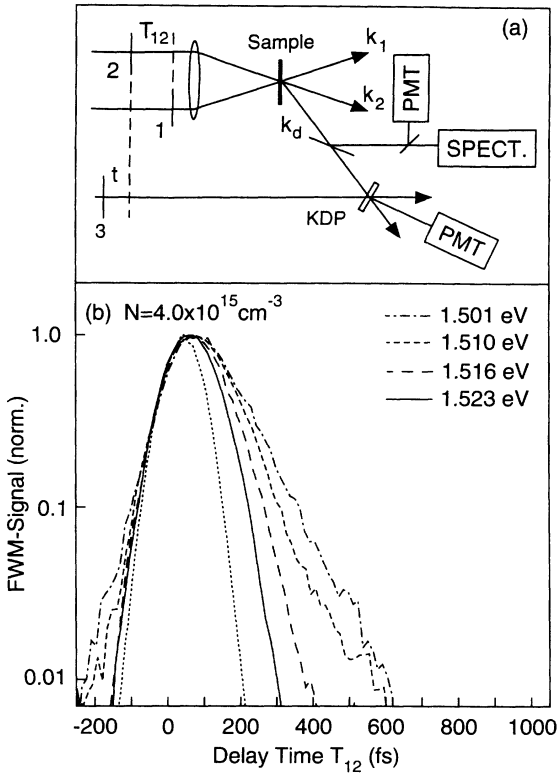

FIG. 1. (a) Schematic of the degenerate FWM experiment. Pulses 1 and 2 create a transient grating in the sample, giving rise to a signal that is spectrally and temporally analyzed (SPECT: monochromator; PMT: photomultipliers). (b) Time evolution of the FWM signal as a function of T_{12}, the delay between pulses 1 and 2. The intensity is plotted on a logarithmic scale for different photon energies of the femtosecond pulses (excitation density 4×10^{15} cm^{-3}). The dotted line is the autocorrelation function of the laser pulses.

II. EXPERIMENTAL TECHNIQUES

Two different samples are studied in our experiments, a 0.5-μm-thick intrinsic and a 0.6-μm-thick p-doped GaAs layer clad by $Al_xGa_{1-x}As$ barriers. The doping concentration of the p-type crystal is 10^{18} cm^{-3}. The GaAs substrates were removed by selective etching to allow for transmission measurements. The experiments with the undoped sample were performed at a lattice temperature of $T_L=10$ K; the p-type material was studied for $T_L=10-120$ K.

Transform-limited pulses of 100-fs duration and a corresponding spectral width of 20 meV (full width at half maximum) are generated with a mode-locked Ti:sapphire laser. The tuning range of this system extends over a wide wavelength interval from 710 to 850 nm with an output power of several hundreds of milliwatts, and a Gaussian intensity distribution across the beam diameter.

The degenerate FWM experiment is depicted schematically in Fig. 1(a). The 100-fs pulses 1 and 2 of identical wavelength generate a transient grating in the sample. The ratio of intensity of the linearly polarized pulses was 1:2. The FWM signal which is emitted by self-diffraction into the direction $\mathbf{k}_d=2\mathbf{k}_2-\mathbf{k}_1$, is studied by the following techniques: (i) The spectrally and temporally integrated intensity is recorded as a function of the delay time T_{12} between pulses 1 and 2. (ii) The FWM signal is spectrally dispersed with the help of a monochromator and detected by a photomultiplier (PMT). The spectral resolution of this experiment was 2 meV. (iii) The temporal envelope is measured with the help of parametric frequency up-conversion.[14] The signal is mixed with a third laser pulse in a nonlinear KDP crystal (thickness 0.5 mm) to generate the sum frequency. Type-II phase matching is used in the up-conversion process to suppress the second harmonic of the laser pulses. The intensity at the sum-frequency recorded as a function of delay time t between the FWM signal and the third laser pulse directly gives the temporal shape of the FWM signal. The excitation densities given below for the different measurements are estimated from the absorption of the sample and the incident flux of laser photons with an accuracy of the absolute values of approximately $\pm50\%$, whereas the relative values are known within $\pm5\%$.

In addition to the FWM studies, the spectra and the time envelope of the excitation pulses transmitted through the samples were recorded to gain insight into possible propagation effects. The measurements show that reshaping of the pulses can be neglected for the optically thin crystals used in the present experiments.

III. EXPERIMENTAL RESULTS

A. Undoped GaAs

First, we study the spectrally and temporally integrated FWM signals. In Fig. 1(b), the intensity diffracted

from the transient grating is plotted as a function of the time delay T_{12} between pulses 1 and 2, generating a total carrier density of 4×10^{15} cm^{-3}. After a fast rise, the signal decays on a subpicosecond time scale, demonstrating the rapid loss of phase coherence (the dotted line is the cross-correlation of pulses 1 and 2). Within the experimental accuracy, the signal follows a monoexponential decay with time constants of $\tau\simeq110$ fs for excitation at or below 1.513 eV, and less than 70 fs at higher photon energies. The intensity of the diffracted signal shows a strong resonant enhancement at the exciton absorption line ($E\simeq1.515$ eV), as was discussed in Ref. 13.

More specific information on the origin of the third order polarization is gained from spectrally resolved FWM signals. First, the FWM spectra for $T_{12}=0$ were studied as a function of carrier density N_{ex} after excitation with femtosecond pulses centered in the free-carrier continuum at $E_{ex}=1.523$ eV.[13] For $N_{ex}\leq10^{16}$ cm^{-3}, we observe a strong excitonic component at 1.513 eV with a spectral width of less than 1/5 of the laser bandwidth. With increasing N_{ex}, this line broadens, and a second contribution occurs around the maximum of the laser spectrum. In should be noted that the carrier densities of our measurements are much lower than in previous femtosecond studies of bulk GaAs.[9-11] This fact illustrates the high sensitivity of our experiment.

In Fig. 2, spectral profiles recorded with $N_{ex}=4\times10^{16}$ cm^{-3} (and a slightly different $E_{ex}=1.531$ eV) are shown for different delay times T_{12}. With increasing T_{12}, the amplitude of the excitonic contribution dominating at delay zero is reduced in comparison to the free-carrier component, resulting in a well-pronounced reshaping of the spectra. In addition, the maximum of the free-carrier part shifts to somewhat smaller photon energies, pointing to a faster dephasing of the free-carrier polarization at higher photon, i.e., carrier energies.

The two components of the nonlinear polarization show a different time behavior which was discussed earlier (see Fig. 2 of Ref. 13). The excitonic polarization at low density exhibits a delayed rise and a decay on a time scale of 1 ps. At higher density, the decay is faster and superimposed at early times by the short pulse-limited signal due to free carriers. For an isolated observation of the two components, the free carrier *or* the excitonic signal selected by interference filters was convoluted with pulse 3.[15] The maximum of the excitonic signal shows a slight shift to earlier times t with increasing delay time T_{12}. A similar behavior is found for the exciton polarization at low densities. In contrast, the free-carrier contribution exhibits a photon-echo-like time behavior with an envelope moving linearly to positive times for increasing delay times T_{12}.

B. *p*-type GaAs

Similar experiments were performed with the *p*-type sample of a high doping concentration of 10^{18} cm^{-3}. The binding energy of the Zn acceptors has a value of approximately 30 meV and—consequently—holes are localized on the impurity atoms at low temperatures. This fact leads to the occurrence of excitons bound to impurities which show a coherent dynamics different from free excitons in the undoped sample. In Fig. 3, the FWM signal from the *p*-doped sample measured at different lattice temperatures T_L is plotted as a function of the delay time T_{12} between the two pulses generating the transient grating (excitation density 10^{16} cm^{-3}). In the individual measurements, the maximum of the laser spectrum, E_{ex}, was

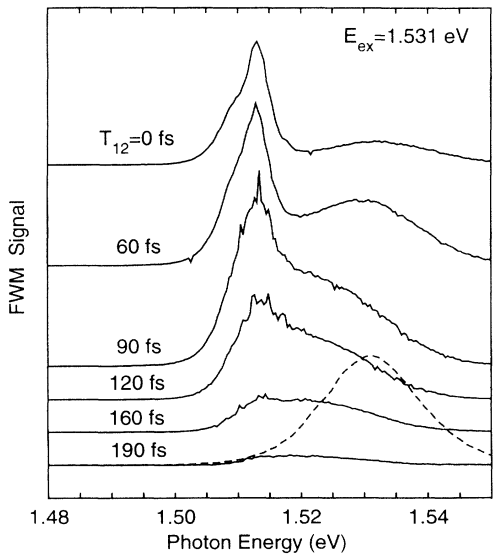

FIG. 2. Spectrally resolved FWM signal for different delay times T_{12} after femtosecond excitation centered at $E_{ex}=1.531$ eV (dashed line: spectrum of the laser pulses). The diffracted intensity is plotted for an excitation density of 4×10^{16} cm^{-3}. An excitonic and a free-carrier component of the optical nonlinearity are observed.

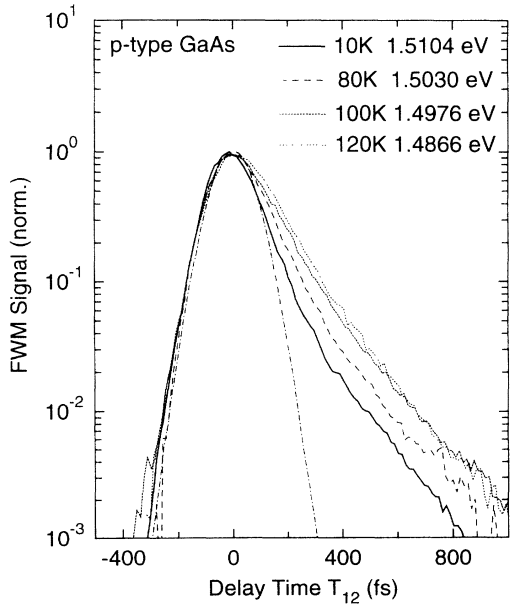

FIG. 3. Femtosecond FWM data for *p*-type GaAs (doping density 10^{18} cm^{-3}). The diffracted intensity is plotted vs delay time T_{12} for different lattice temperatures T_L. The excitation pulses creating 10^{16} carriers per cm^{-3} are resonant to the band edge at the different temperatures.

adjusted to the temperature-dependent position of the band edge. We observe a decay of the coherent polarization that is slower than in the case of the undoped sample.

For $E_{ex}=1.51$ eV ($T_L=10$ K), the spectrally resolved FWM signal mainly shows an excitonic line around 1.512 eV. The full width at half maximum of this spectrum broadens from 2 meV at an excitation density of $N_{ex}=3\times10^{14}$ cm^{-3} to 10 meV at $N_{ex}=10^{16}$ cm^{-3}. This increase of linewidth reflects the faster dephasing of the polarization at a higher carrier concentration.

With increasing temperature, a substantial fraction of acceptors is ionized, giving rise to an additional absorption band, the acceptor deionization band. This absorption, which is located below the fundamental absorption edge, is due to transitions from negatively charged acceptor ions to the conduction band. A possible contribution of those transitions to the FWM signals was investigated with excitation pulses in the relevant spectral range. However, even for temperatures as high as 120 K, the spectrum of the diffracted intensity shows exclusively excitonic features.

The time envelope of the diffracted intensity was determined with the help of the up-conversion technique. The transients in Figs. 4(a)–4(e) are observed for an excitation density of $N_{ex}=6\times10^{15}$ cm^{-3}. The excitation pulses are centered at $E_{ex}=1.51$ eV, close to the maximum of the FWM spectra (lattice temperature $T_L=10$ K). The signal exhibits two clearly separated components at early and at late delay times. In comparison to the intrinsic sample, the time-resolved data show a slower decay of coherent polarization that persists well in the picosecond regime.

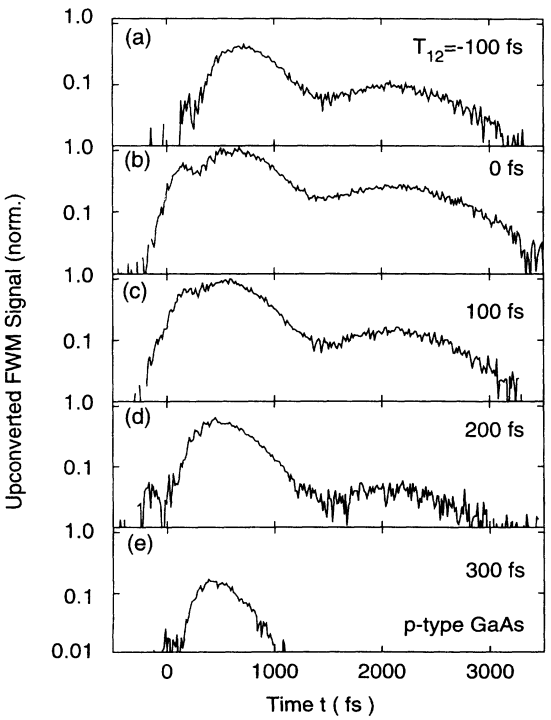

FIG. 4. (a)–(e) Temporal profiles of the FWM signals from p-type GaAs. The upconverted intensity is plotted vs delay time t between pulses 2 and 3 for different values of T_{12}. Two clearly separated components of the signal are observed.

IV. DISCUSSION

We now present a qualitative discussion of the experimental results that is complemented by the detailed theoretical analysis in Sec. V. The bandwidth of the 100-fs pulses has a value of 20 meV which is substantially larger than the excitonic binding energy of 4.2 meV. For laser pulses with maximum at about 1.523 eV, both excitonic *and* free-carrier states are excited in the undoped sample and contribute to the overall nonlinear polarization of the material. The spectrum of the excitation pulses overlaps with a broad interval of continuum states, whereas the excitonic polarization is driven with a small fraction of the incident power. Nevertheless, the spectrally resolved data for carrier densities below 10^{16} cm^{-3} show a very strong excitonic enhancement compared to which the free-carrier polarization is negligible. This finding is due to (i) the large ratio $(d_{ex}/d_{con})\simeq10$ of the excitonic (d_{ex}) and interband (d_{con}) oscillator strengths,[16–18] and (ii) to the slow dephasing of the excitonic polarization which persists considerably longer than the free-carrier contribution.[13] For densities above 10^{16} cm^{-3}, excitonic and free-carrier contributions are of similar strengths. With increasing concentration of free electrons and holes, screening of their attractive interaction lowers the ionization continuum of excitons, leading to a decrease of the excitonic oscillator strength and of the resonant enhancement.

A similar enhancement due to bound excitons is found in the p-type sample, where the excitonic dephasing is even slower than in the undoped material. Both interband transitions and the acceptor deionization band are of much smaller oscillator strengths, and make minor contributions to the observed nonlinear polarization near the band edge.

With increasing time delay T_{12} between the pulses forming the grating, a well-pronounced reshaping of the FWM spectra is observed. The undoped sample shows the following behavior (Fig. 2): (i) The free-carrier contribution is redshifted for long delay times. The polarization components at high photon, i.e., electron and hole energies follow a very fast dephasing kinetics and—thus—disappear in the spectrum of the coherent signal more rapidly than the low-energy contributions. Enhanced rates of carrier-carrier scattering, which governs this ultrafast dephasing, are favored by the larger density of final states for the scattering partners at higher energies. (ii) The relative amplitude of the excitonic component is reduced with increasing delay time T_{12}. This fact points to the loss of electron-hole correlation by carrier redistribution occurring during and immediately after the first excitation pulse.

Information about the temporal behavior of nonlinear polarization is obtained from the data in Figs. 1 and 3, where the diffracted intensity was measured as a function of the delay between the pulses 1 and 2, generating the transient grating in the samples. For a carrier density of 4×10^{15} cm^{-3} in undoped GaAs, the dephasing rates of the essentially excitonic polarization increase for the

higher photon energy of the excitation pulses. Tuning the laser to higher photon energies reduces the overlap of the spectrum with the excitonic line and leads to a stronger excitation of continuum states. In this way, dephasing of the exciton transition by collisions with free carriers is enhanced, resulting in a faster decay of the time-integrated signal.

The temporal properties of the nonlinear polarization were studied more directly in a second series of experiments where the time envelope of the diffracted intensity was measured. In principle, the time-dependent electric field of this signal can be calculated from the frequency-dependent field by Fourier analysis if the amplitude and phase of the spectrally resolved signal is known. However, this and other spectrally resolved studies[7] give the power spectrum of the FWM signal where the phase information is lost, and—consequently—an unambiguous transformation to the time domain is not possible. Thus the time-resolved detection of the diffracted intensity in our experiments provides direct independent information about the temporal characteristics of the nonlinear polarization.[19]

The time-resolved data reported in Ref. 13 demonstrate the distinctly different temporal behavior of the two parts of the nonlinear polarization. The free-carrier states optically coupled by the femtosecond pulses represent an inhomogeneously broadened ensemble giving rise to a photon echo. The loss of phase coherence by carrier-carrier collisions results in a decay time which is shorter than our time resolution of about 70 fs. For an excitation density of 4×10^{16} cm^{-3}, a reduction of the scattering rates by Pauli blocking of electronic states is negligible in our nonequilibrium situation. In contrast, the experiments of Ref. 9, giving T_2 times around 300 fs, were performed at much higher densities where those effects might be important.

The excitonic signal has a more complicated temporal structure. For the undoped sample, we observe a time envelope with a single maximum. With increasing T_{12}, the latter shifts slightly toward earlier times t. A different time behavior is found for the polarization due to bound excitons in the p-doped crystal which show a slower dephasing kinetics. The data in Fig. 4 exhibit two clearly separated contributions, a prompt component with maximum at early delay times and a delayed signal that peaks after approximately 2 ps.

The shape of the excitonic signals is strongly influenced by many body effects among the carriers which are coupled via the Coulomb interaction.[4,6,12,20] Recent studies of excitons in GaAs/$Al_xGa_{1-x}As$ quantum wells revealed a prompt signal due to phase-space filling (PSF) that is emitted immediately after pulse 2; i.e., it shows a maximum at early times. A second component due to exciton-exciton interaction (EEI) peaks at later times $t\simeq T_2$.[4,6] For the short dephasing times T_2 occurring in the undoped sample after excitation of exciton and continuum states, superposition of the two contributions gives a broad time envelope with a single maximum as observed in our measurements. In contrast, the slower dephasing of bound excitons in the p-type crystal allows the distinction of prompt and delayed components.

The relative strength of the PSF component rises with increasing T_{12}. In the undoped sample, this fact is obvious from the small shift of the temporal envelope toward smaller times t and the corresponding decrease of excitonic enhancement in the FWM spectra (Fig. 2). For the p-type material, the amplitude of the second (EEI) maximum relative to the first (PSF) one (see Fig. 4) is considerably reduced with increasing delay T_{12}.

V. THEORETICAL ANALYSIS

A. Theoretical model

The experiments were analyzed by a numerical solution of the semiconductor Bloch equations for the FWM geometry using the Fourier expansion described in Ref. 12. By neglecting effects of spatial transport, the basic quantities for the dynamics, i.e., the distribution functions of electrons and holes and the interband polarization, can be parametrized by a spatial coordinate R. The spatial inhomogeneity is introduced by the two laser pulses traveling in the directions $\mathbf{k}_1$ and $\mathbf{k}_2$. With $\mathbf{k}_1=\mathbf{Q}+\mathbf{q}$ and $\mathbf{k}_2=\mathbf{Q}-\mathbf{q}$, the external field described in terms of its vector potential $A(t)=2\,\mathrm{Re}\,A^{(+)}(t)$ is given by

$$A^{(+)}(t)=[A_0^{(1)}(t)e^{i\mathbf{q}\cdot\mathbf{R}}+A_0^{(-1)}(t)e^{-i\mathbf{q}\cdot\mathbf{R}}]e^{i(\mathbf{Q}\cdot\mathbf{R}-\omega_L t)} \tag{1}$$

and $A^{(-)}(t)=A^{(+)*}(t)$, where $A_0^{(+1)}(t)$ and $A_0^{(-1)}(t)$ denote the temporal shapes of the laser pulses here taken to be Gaussian. Inserting a Fourier expansion of the distribution functions according to

$$f_{\mathbf{k}}^{e,h}=\sum_{n=-\infty}^{\infty}f_{\mathbf{k}}^{e,h(n)}e^{in\mathbf{q}\cdot\mathbf{R}}\,, \tag{2}$$

and of the polarization according to

$$p_{\mathbf{k}}=e^{i\mathbf{Q}\cdot\mathbf{R}}\sum_{n=-\infty}^{\infty}p_{\mathbf{k}}^{(n)}e^{in\mathbf{q}\cdot\mathbf{R}} \tag{3}$$

in the semiconductor Bloch equations, leads to a coupled set of equations for the Fourier components where only the even contributions of the distribution functions and the odd components of the polarization remain. Restricting ourselves to the lowest order necessary to describe a FWM experiment, we take $f_{\mathbf{k}}^{e,h(0)}$ describing the homogeneous part of the carrier distribution, $f_{\mathbf{k}}^{e,h(2)}=f_{\mathbf{k}}^{e,h(-2)}$ describing the transient grating, $p_{\mathbf{k}}^{(1)}$ and $p_{\mathbf{k}}^{(-1)}$ describing the polarizations in the directions of the two pulses, and $p_{\mathbf{k}}^{(3)}$ and $p_{\mathbf{k}}^{(-3)}$ describing the diffracted polarizations. We introduce the effective field $U_{\mathbf{k}}=M_{\mathbf{k}}A^{(+)}(t)+\Delta_{\mathbf{k}}$, where

$$\Delta_{\mathbf{k}}=-\sum_{\mathbf{k}'}V_{\mathbf{k}-\mathbf{k}'}p_{\mathbf{k}'} \tag{4}$$

is the internal field in the Hartree-Fock approximation, and the corresponding Fourier expansion is

$$U_{\mathbf{k}}=e^{i\mathbf{Q}\cdot\mathbf{R}}\sum_{n=-\infty}^{\infty}U_{\mathbf{k}}^{(n)}e^{in\mathbf{q}\cdot\mathbf{R}}\,. \tag{5}$$

The equations of motion for the Fourier components of the distribution functions are given by

$$\frac{d}{dt}f_{\mathbf{k}}^{e(0)}=\frac{1}{i\hbar}[U_{\mathbf{k}}^{(1)}p_{\mathbf{k}}^{(1)*}+U_{\mathbf{k}}^{(3)}p_{\mathbf{k}}^{(3)*}+U_{\mathbf{k}}^{(-1)}p_{\mathbf{k}}^{(-1)*}+U_{\mathbf{k}}^{(-3)}p_{\mathbf{k}}^{(-3*)}-\text{c.c.}]+\sum_{\mathbf{k}'}[W_{\mathbf{k}\mathbf{k}'}f_{\mathbf{k}'}^{e(0)}-W_{\mathbf{k}'\mathbf{k}}f_{\mathbf{k}}^{e(0)}]\ , \tag{6}$$

$$\frac{d}{dt}f_{\mathbf{k}}^{e(2)}=\frac{1}{i\hbar}[U_{\mathbf{k}}^{(3)}p_{\mathbf{k}}^{(1)*}+U_{\mathbf{k}}^{(1)}p_{\mathbf{k}}^{(-1)*}+U_{\mathbf{k}}^{(-1)}p_{\mathbf{k}}^{(-3)*}-U_{\mathbf{k}}^{(1)*}p_{\mathbf{k}}^{(3)}-U_{\mathbf{k}}^{(-1)*}p_{\mathbf{k}}^{(1)}-U_{\mathbf{k}}^{(-3)*}p_{\mathbf{k}}^{(-1)}]$$
$$+\sum_{\mathbf{k}'}[W_{\mathbf{k}\mathbf{k}'}f_{\mathbf{k}'}^{e(2)}-W_{\mathbf{k}'\mathbf{k}}f_{\mathbf{k}}^{e(2)}]\ . \tag{7}$$

The equations of motion for the Fourier components of the polarizations are

$$\frac{d}{dt}p_{\mathbf{k}}^{(1)}=\frac{1}{i\hbar}[(\epsilon_{\mathbf{k}}^{e}+\epsilon_{-\mathbf{k}}^{h}+\Omega_{\mathbf{k}})p_{\mathbf{k}}^{(1)}+U_{\mathbf{k}}^{(1)}(1-f_{\mathbf{k}}^{e(0)}-f_{-\mathbf{k}}^{h(0)})-U_{\mathbf{k}}^{(3)}(f_{\mathbf{k}}^{e(-2)}+f_{-\mathbf{k}}^{h(-2)})-U_{\mathbf{k}}^{(-1)}(f_{\mathbf{k}}^{e(2)}+f_{-\mathbf{k}}^{h(2)})]-\frac{1}{\hbar}\Gamma_{\mathbf{k}}p_{\mathbf{k}}^{(1)}\ , \tag{8}$$

$$\frac{d}{dt}p_{\mathbf{k}}^{(3)}=\frac{1}{i\hbar}[(\epsilon_{\mathbf{k}}^{e}+\epsilon_{-\mathbf{k}}^{h}+\Omega_{\mathbf{k}})p_{\mathbf{k}}^{(3)}+U_{\mathbf{k}}^{(3)}(1-f_{\mathbf{k}}^{e(0)}-f_{-\mathbf{k}}^{h(0)})-U_{\mathbf{k}}^{(1)}(f_{\mathbf{k}}^{e(2)}+f_{-\mathbf{k}}^{h(2)})]-\frac{1}{\hbar}\Gamma_{\mathbf{k}}p_{\mathbf{k}}^{(1)}\ , \tag{9}$$

and the equations for $p_{\mathbf{k}}^{(-1)}$ and $p_{\mathbf{k}}^{(-3)}$ are obtained from Eqs. (8) and (9) by changing signs in the superscripts denoting the Fourier components. Here $\Omega_{\mathbf{k}}$ and $\Gamma_{\mathbf{k}}$ denote the real and imaginary part of the carrier self-energy, and $W_{\mathbf{k}\mathbf{k}'}$ is the scattering rate from state $\mathbf{k}'$ to $\mathbf{k}$. We have neglected an additional coupling of the Fourier components due to the space dependence in the self-energy screening and the scattering rate. These quantities are calculated only with the homogeneous parts $f_{\mathbf{k}}^{e,h(0)}$ of the distribution functions. The real part of the self-energy is given by the screened exchange and the Coulomb hole energy,[17] and the following scattering mechanisms have been included: carrier-carrier scattering in the static screening approximation; and scattering with phonons via the polar-optical interaction and with acoustic phonons via deformation-potential coupling. The imaginary part of the self-energy strongly overestimates the dephasing due to small-angle scattering by assuming a loss of phase coherence independent of the scattering angle. To avoid this problem, we have modeled the dephasing contribution due to carrier-carrier scattering by a constant rate Γ_{cc}.

Equations (5)–(9) were solved numerically by the technique described in Ref. 21. The Monte Carlo algorithm used for the calculation of the distribution function has been generalized to allow for the complex functions $f_{\mathbf{k}}^{e,h(2,-2)}$. Due to the positive scattering rates $W_{\mathbf{k}\mathbf{k}'}$, the collision term in Eq. (7) does not mix real and imaginary parts, which both can be calculated separately. The positive and negative contributions in each part are incorporated by performing simulations in which the carriers are weighted either by $+1$ if the function is positive, or -1 if it is negative.

B. Results of the simulation

In Fig. 5(a), the spectrally resolved FWM signal at time delay $T_{12}=0$ is plotted for different densities. The dephasing rate due to carrier-carrier interaction has been chosen as $\Gamma_{cc}=1/T_2=2\ \text{ps}^{-1}$. As observed in the experiment, the signal is concentrated at the exciton up to a density of $10^{16}\ \text{cm}^{-3}$. A free-carrier contribution centered at the energy of the incident pulses appears and increases with increasing density. The overall agreement with the experiment is very good. However, we find some slight differences: In contrast to the experiments, the calculated spectra exhibit a redshift with increasing density which is not found in the measurements. This redshift has been found also in quasiequilibrium spectra at high densities.[22] Furthermore, the free-carrier contribution begins to dominate at somewhat lower densities than in the experiments. We attribute this difference mainly to limitations of the static screening model used in the calculations. Even at quasiequilibrium it has been found that the static limit overestimates the screening. Under nonequilibrium conditions, such as is in the present study, dynamic aspects of the screening become more important.[23–25] In the case of ultrafast processes,

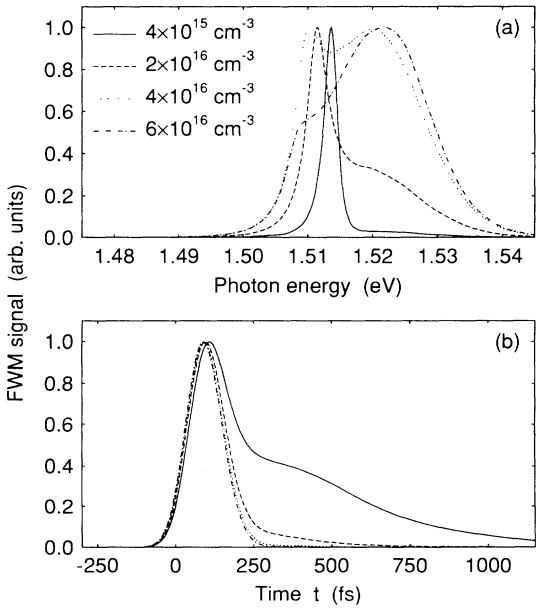

FIG. 5. (a) Spectrally and (b) temporally resolved FWM signals at delay zero $T_{12}=0$ for different carrier densities as obtained from the numerical calculations.

even a dielectric function depending on frequency becomes questionable, and a full model should be based on a dielectric function which depends explicitly on two times in order to describe the correct buildup of the screening.[26–28] Such models, however, have not yet been included in full numerical solutions of the semiconductor Bloch equations for a FWM experiment.

Figure 5(b) shows the corresponding time-resolved up-converted signals. As already discussed in Refs. 12 and 20, the signal consists of two parts: a prompt part related to the free-carrier dynamics and a delayed part related to the excitonic contribution. As in the spectrally resolved signal, the excitonic contribution decreases with increasing density. It is interesting to notice that at densities where an excitonic contribution is still clearly visible in the spectrally resolved signal, the time-resolved curve exhibits practically only free-carrier contributions. Thus spectrally resolved measurements are more sensitive in this density range.

The results in Fig. 6 demonstrate the influence of the dephasing rate on the spectrum and on the time-resolved signals for two different densities at zero delay. In the low-density case [Fig. 6(a)], the spectrum is always concentrated at the exciton energy. The decreasing linewidth directly reflects the decreasing dephasing rate. In the high-density case [Fig. 6(b)], we see that the relative height of the exciton and the free-carrier contribution depends strongly on the dephasing rate. A decreasing rate leads to an increase in the excitonic contribution.

While in the spectra the changes are more pronounced in the high-density case, the time-resolved signals exhibit the opposite behavior. In the high-density case [Fig. 6(d)], the signal seems to be nearly independent of the dephasing rate. Only the delayed part, which is nearly invisible in this linear plot, is modified. On the other hand, this change in the delayed part is clearly visible for low carrier densities [Fig. 6(c)]. We observe a shift of the maximum toward later times, and the appearance of more complicated envelopes with decreasing dephasing rate. This is in qualitative agreement with the experimental results measured with the *p*-type sample, where the dephasing times were longer than in the undoped case. A similar behavior was reported for excitonic polarizations in quasi-two-dimensional semiconductors.[6]

In Fig. 7, we show the calculated spectrally and temporally resolved FWM signal for a density of $N=4\times10^{16}$ cm^{-3} at various delay times. For increasing negative delay, there is an increasing excitonic peak. This behavior is due to the fact that at negative delay times, i.e., with no temporal overlap of the two pulses, no signal can be directly diffracted into the observed direction. Thus only many-body effects lead to a signal.[1,29] This increase in the excitonic part of the spectrum is connected with an increasing delayed contribution in the time-resolved signal. With increasing positive delay, the excitonic contribution decreases and the time-resolved signals show a clear photon-echo behavior.

After discussing the dynamics of the nonlinear polarization that gives rise to the FWM signal, let us now turn to the dynamics of the various components of the distribution functions. In Figs. 8 and 9, we have plotted the energy distributions $F^{e,h,(n)}$ which are obtained by multiplying the distribution functions $f_{\mathbf{k}}^{e,h(n)}$ by the density of states. This distribution gives a more intuitive picture of the relaxation process since its area is directly proportional to the carrier density. Figure 8 shows the electron and hole distributions at zero delay. For all times after the pulses, the distribution functions are essentially thermalized. The electron distributions exhibit a cooling, while the hole distributions show a heating with increasing time. This behavior is due to the fact that the excess energy of electrons supplied by the laser pulses is higher

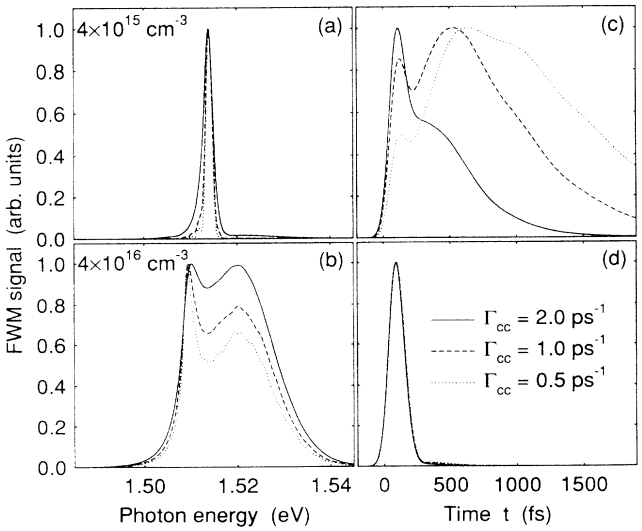

FIG. 6. Influence of the carrier dephasing rate on the (a) and (b) spectrally and (c) and (d) temporally resolved FWM signals calculated for $T_{12}=0$. Results are plotted for excitation densities of 4×10^{15} and 4×10^{16} cm^{-3}.

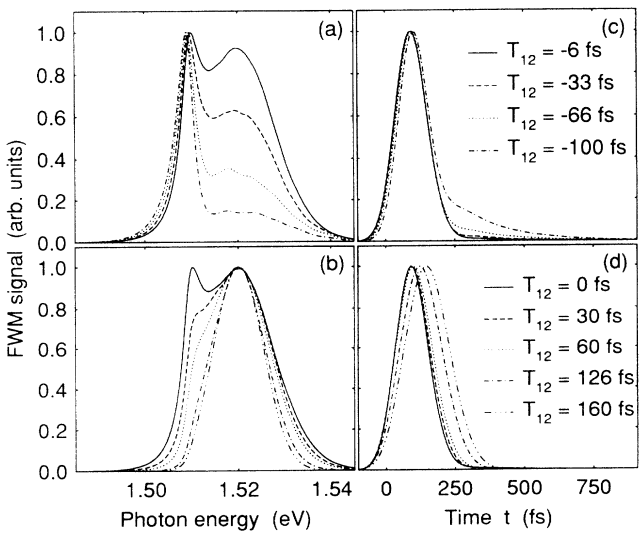

FIG. 7. (a) and (b) spectrally and (c) and (d) temporally resolved FWM signals as calculated from the theoretical model. Results are shown for negative (a) and (c) and positive (b) and (d) delay times T_{12}. The carrier density is 4×10^{16} cm^{-3}.

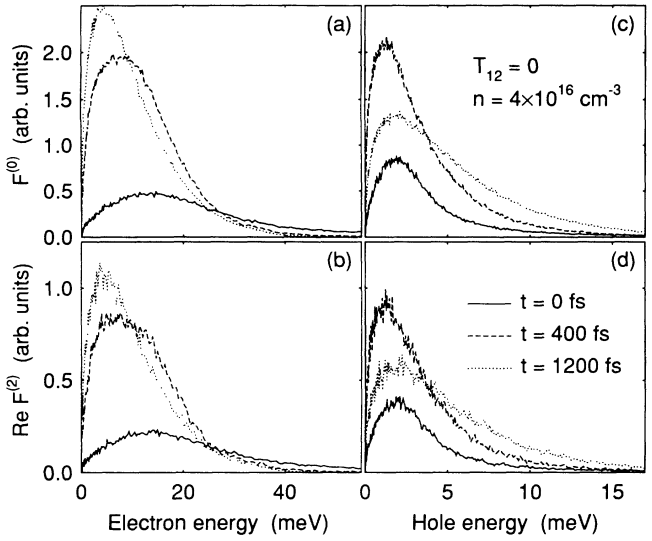

FIG. 8. Energy distributions of (a) and (b) electrons and (c) and (d) holes (weighted by the densities of states) for an excitation density 4×10^{16} cm^{-3} and zero delay $T_{12}=0$ between pulses 1 and 2. Distributions are plotted for different times t after the maxima of pulses 1 and 2. The homogeneous parts of the distributions, $F^{(0)}$, are shown in (a) and (c), whereas (b) and (d) give the real parts of the transient grating, Re($F^{(2)}$). The imaginary parts of the transient grating vanish.

than the hole energy. The main mechanism for the energy exchange is inelastic electron-hole scattering. However, even for the small excess energy of the laser of only 4 meV, there is a significant emission of optical phonons by the electrons. At early delay times, a substantial fraction of the electrons populates states above the threshold for optical-phonon emission at 36.4 meV. This contribution has mainly two origins: First, it is related simply to the

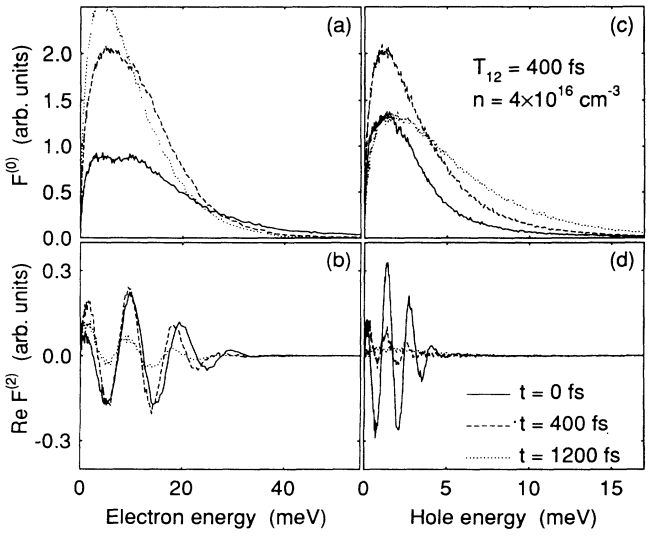

FIG. 9. Same as Fig. 8 for a time delay $T_{12}=400$ fs. The imaginary parts of the transient grating have a similar shape as the real parts in (b) and (d).

density of states which results in a higher weight of the high-energy tail of the laser spectrum compared to the low-energy tail. Second, as discussed in detail in Ref. 21, the broadening of the generation rate during the pulse is larger than that which one estimates from the energy-time uncertainty relation leading to an additional increase in the high-energy tail of the distribution.

The real part of the transient grating contribution $F^{e,h(2)}$ for electrons as well as holes has the same shape and a magnitude of somewhat less than half of the homogeneous contribution $F^{e,h(0)}$. The imaginary parts of $F^{e,h(2)}$ are practically zero, reflecting the fact that for zero delay the two pulses create an interference pattern proportional to $\cos(\mathbf{k}_2-\mathbf{k}_1)\mathbf{r}$. The magnitude is less than one half, because the amplitudes of the two laser pulses have been taken different by a factor of 1.5, in agreement with the experimental conditions.

In Fig. 9, the distribution functions are shown at a delay time of 400 fs. The homogeneous parts of the distribution functions are essentially the same, only at $t=0$ there are slight differences since the carriers generated by the first pulse have partly relaxed, thus increasing the low-energy part of the distribution. Furthermore, the densities are different since for zero delay half of the final carrier density exists at $t=0$, whereas about $\frac{3}{4}$ of the final density are already created for nonoverlapping pulses. The transient grating part, however, is completely different. For finite delay, the grating is created by the interference between the second pulse and the polarization left over from the first pulse. Here we are in the limit of inhomogeneous broadening in k space. Different $\mathbf{k}$ contributions of the polarization have different frequencies leading to different phase shifts of the transient grating. The real as well as imaginary parts of $F^{e,h(2)}$ (which is similar to the plotted real part) show oscillations in $\mathbf{k}$ space. The scattering processes destroy the gratings because of these oscillations, in contrast to the case of zero delay. In particular, the hole distribution is completely homogeneous after about 800 fs without any spatial transport. In the case of electrons, this smoothing is somewhat slower, but the spatial modulation of electron density is reduced to a few percent around the average distribution after 1.2 ps.

Theoretical calculations and experimental studies of the absorption spectra of bulk GaAs give a (Mott) density $N_c\simeq4\times10^{15}$ cm^{-3} of thermalized free carriers at a temperature of 10 K for which the exciton ground state merges into the continuum.[16,17] Our FWM spectra, however, show excitonic contributions up to $N_{ex}\simeq6\times10^{16}$ cm^{-3}, much higher than N_c. This behavior is caused by the very broad, initially nonthermal distributions of electrons and holes which screen the attractive e-h interaction less effectively than in the case of an equilibrium distribution.

VI. CONCLUSIONS

In conclusion, the results presented here give detailed insight into the nonlinear polarization of undoped and p-doped GaAs occurring after simultaneous excitation of excitonic and free-carrier states. Spectrally and tem-

porally resolved four-wave-mixing studies, in which the material is excited close to the band gap by laser pulses of 100-fs duration, reveal an excitonic nonlinearity that dominates in both samples for carrier densities below 10^{16} cm^{-3}. The temporal profile of the excitonic polarization is determined by many-body effects in the carrier system, and consists of an instantaneous contribution and a delayed component with maximum at $t \simeq T_2$. At carrier concentrations higher than 10^{16} cm^{-3}, electrons and holes in continuum states reduce the excitonic contribution via screening, and give rise to an additional component of similar strength that shows a spectral profile resonant to the laser pulses. The transient reshaping of this spectrum demonstrates different dephasing kinetics of continuum states excited by low- and high-energy parts of the laser spectrum. A photon-echo-like time behavior is observed for the free-carrier polarization. The experiments were combined with theoretical calculations comprising the numerical solutions of the Bloch equations (including many-body effects) and an ensemble Monte Carlo simulation of the underlying carrier dynamics. The calculated coherent polarizations and FWM signals are in quantitative agreement with spectrally and temporally resolved data. Furthermore, the different components of the transient carrier distribution function are obtained from the simulation, revealing electron and hole thermalization by carrier-carrier collisions on a time scale of 200 fs.

[1]K. Leo, M. Wegener, J. Shah, D. S. Chemla, E. O. Göbel, T. C. Damen, S. Schmitt-Rink, and W. Schäfer, Phys. Rev. Lett. **65**, 1340 (1990).

[2]M. Wegener, D. S. Chemla, S. Schmitt-Rink, and W. Schäfer, Phys. Rev. A **42**, 5675 (1990).

[3]M. D. Webb, S. T. Cundiff, and D. G. Steel, Phys. Rev. Lett. **66**, 934 (1991).

[4]S. Weiss, M.-A. Mycek, J.-Y. Bigot, S. Schmitt-Rink, and D. S. Chemla, Phys. Rev. Lett. **69**, 2685 (1992).

[5]J. Y. Bigot, M. A. Mycek, S. Weiss, R. G. Ulbrich, and D. S. Chemla, Phys. Rev. Lett. **70**, 3307 (1993).

[6]D. S. Kim, J. Shah, T. C. Damen, W. Schäfer, F. Jahnke, S. Schmitt-Rink, and K. Köhler, Phys. Rev. Lett. **69**, 2725 (1992).

[7]T. Rappen, U. Peter, M. Wegener, and W. Schäfer, Phys. Rev. B **48**, 4879 (1993).

[8]L. Schultheis, J. Kuhl, A. Honold, and C. W. Tu, Phys. Rev. Lett. **57**, 1635 (1986); **57**, 1797 (1986).

[9]J. L. Oudar, D. Hulin, A. Migus, A. Antonetti, and F. Alexandre, Phys. Rev. Lett. **55**, 2074 (1985).

[10]M. T. Portella, J.-Y. Bigot, R. W. Schoenlein, J. E. Cunningham, and C. V. Shank, Appl. Phys. Lett. **60**, 2123 (1992).

[11]P. C. Becker, H. L. Fragnito, C. H. BritoCruz, R. L. Fork, J. E. Cunningham, J. E. Henry, and C. V. Shank, Phys. Rev. Lett. **61**, 1647 (1988).

[12]M. Lindberg, R. Binder, and S. W. Koch, Phys. Rev. A **45**, 1865 (1992).

[13]A. Lohner, K. Rick, P. Leisching, A. Leitenstorfer, T. Elsaesser, T. Kuhn, F. Rossi, and W. Stolz, Phys. Rev. Lett. **71**, 77 (1993).

[14]J. Shah, IEEE J. Quantum Electron. **24**, 276 (1988).

[15]Spectral filtering results in a temporal broadening of the signal of less than 50 fs, i.e., short compared to the pulse duration.

[16]R. G. Ulbrich, in *Optical Nonlinearities and Instabilities in Semiconductors,* edited by H. Haug (Academic, New York, 1988), p. 121.

[17]H. Haug and S. Schmitt-Rink, Prog. Quantum Electron. **9**, 3 (1984).

[18]D. S. Kim, J. Shah, J. E. Cunningham, T. C. Damen, W. Schäfer, M. Hartmann, and S. Schmitt-Rink, Phys. Rev. Lett. **68**, 1006 (1992).

[19]Phase-sensitive FWM experiments have been reported in Ref. 5.

[20]W. Schäfer, F. Jahnke, and S. Schmitt-Rink, Phys. Rev. B **47**, 1217 (1993).

[21]T. Kuhn and F. Rossi, Phys. Rev. Lett. **69**, 977 (1992); Phys. Rev. B **46**, 7496 (1992).

[22]H. Haug and S. W. Koch, *Quantum Theory of the Optical and Electronic Properties of Semiconductors,* 2nd ed. (World Scientific, Singapore, 1993).

[23]T. Elsaesser, J. Shah, L. Rota, and P. Lugli, Phys. Rev. Lett. **66**, 1757 (1991).

[24]L. Rota, P. Lugli, T. Elsaesser, and J. Shah, Phys. Rev. B **47**, 4226 (1993).

[25]D. C. Scott, R. Binder, and S. W. Koch, Phys. Rev. Lett. **69**, 347 (1992).

[26]M. Hartmann, H. Stolz, and R. Zimmermann, Phys. Status Solidi B **159**, 35 (1989).

[27]H. Haug and C. Ell, Phys. Rev. B **46**, 2126 (1992).

[28]D. B. TranThoai and H. Haug, Z. Phys. B **91**, 199 (1993).

[29]C. Stafford, S. Schmitt-Rink, and W. Schäfer, Phys. Rev. B **41**, 10 000 (1990).